NeuroImage 218 (2020) 116974

Contents lists available at ScienceDirect

NeuroImage

journal homepage: www.elsevier.com/locate/neuroimage

The modular organization of brain cortical connectivity across the human lifespan

Maria Grazia Puxeddu [a,b,*], Joshua Faskowitz [c,d], Richard F. Betzel [c,d,e,f], Manuela Petti [a,b], Laura Astolfi [a,b,1], Olaf Sporns [c,d,e,f,1]

[a] Department of Computer, Control and Management Engineering, University of Rome La Sapienza, Rome, 00185, Italy
[b] IRCSS, Fondazione Santa Lucia, Rome, 00142, Italy
[c] Program in Neuroscience, Indiana University, Bloomington, IN, USA
[d] Department of Psychological and Brain Sciences, Indiana University, Bloomington, IN, USA
[e] Cognitive Science Program, Indiana University, Bloomington, IN, USA
[f] Indiana University Network Science Institute, Indiana University, Bloomington, IN, USA

ARTICLE INFO

Keywords:
Connectome
Lifespan
Multilayer networks
Modularity

ABSTRACT

The network architecture of the human brain contributes in shaping neural activity, influencing cognitive and behavioral processes. The availability of neuroimaging data across the lifespan allows us to monitor how this architecture reorganizes, influenced by processes like learning, adaptation, maturation, and senescence. Changing patterns in brain connectivity can be analyzed with the tools of network science, which can be used to reveal organizational principles such as modular network topology. The identification of network modules is fundamental, as they parse the brain into coherent sub-systems and allow for both functional integration and segregation among different brain areas. In this work we examined the brain's modular organization by developing an ensemble-based multilayer network approach, allowing us to link changes of structural connectivity patterns to development and aging. We show that modular structure exhibits both linear and nonlinear age-related trends. In the early and late lifespan, communities are more modular, and we track the origins of this high modularity to two different substrates in brain connectivity, linked to the number and the weights of the intra-clusters edges. We also demonstrate that aging leads to a progressive and increasing reconfiguration of modules and a redistribution across hemispheres. Finally, we identify those brain regions that most contribute to network reconfiguration and those that remain more stable across the lifespan.

1. Introduction

The human brain is a complex system that can be modeled as a network of anatomically interconnected brain regions, referred to as the *connectome* (Bullmore and Sporns, 2009; Sporns, 2011). Modeling the brain as a network allows the use of graph theory tools to explore properties of brain connectivity (Bassett and Sporns, 2017), through which we can enhance our understanding of neurocognitive function and better characterize neurobiological variation across subjects or clinical populations (Kelly et al., 2012; Sporns, 2014). Network neuroscience approaches also allow for the tracking of networks across time, across different developmental stages, and in aging. Previous studies have shown that the brain and white matter connectivity exhibits characteristic changes across the human lifespan (Imperati et al., 2011; Lebel et al., 2012; Westlye et al., 2010; Yeatman et al., 2014), as well as specific changes in connectivity during adolescent development (Byrge et al., 2014; Di Martino et al., 2014), adulthood (Duffau, 2014), and senescence (Andrews-Hanna et al., 2007; Buckner et al., 2009; Filippi et al., 2013; Zhou et al., 2012). New efforts, made possible by large multi-modal neuroimaging datasets, have focused on charting brain networks across the entire human lifespan. This approach is meant to help in better understanding developmental processes and the age-related decline of executive and cognitive function.

Recent cross-sectional studies (for review see (Zuo et al., 2017)) have already applied complex network tools to evaluate local and global changes in the connectome during the lifespan. For example in (Betzel

* Corresponding author. Department of Computer Control and Management Engineer, University of Rome La Sapienza, Via Ariosto 25, 00185, Rome, Italy.
E-mail address: puxeddu@diag.uniroma1.it (M.G. Puxeddu).
[1] Laura Astolfi and Olaf Sporns should be considered joint senior author.

https://doi.org/10.1016/j.neuroimage.2020.116974
Received 11 October 2019; Received in revised form 17 February 2020; Accepted 17 May 2020
Available online 22 May 2020

et al., 2014; Lim et al., 2015) an age-related decrease in the number of recovered connections between brain areas has been recorded. In (Sinke et al., 2016) and (Petti et al., 2016) other topological features like local clustering and global efficiency have been investigated by means of different neuroimaging techniques. However, few attempts have been made to characterize how the connectome's community structure (Fortunato, 2010; Newman, 2012; Porter et al., 2009), a hallmark of complex networks, evolves across the lifespan. Community structure is expressed at a mesoscale level (Betzel and Bassett, 2017) (between local and global) allowing observations on how the network's units organize themselves into clusters (communities) to form coherent and distributed systems that balance integration and segregation between brain regions. While different definitions of communities exist (Betzel et al., 2018b; Schaub et al., 2017), it is well established that anatomical brain networks exhibit assortative communities (Bassett et al., 2011a; Sporns and Betzel, 2016), called modules. Modular structure implies the presence of different internally dense and externally sparse subnetworks, usually related to specific domains of brain function. Studies on functional connectivity have found an age-related increase in between-module connectivity and a decrease in within-module connectivity (Betzel et al., 2014; Chan et al., 2014), plus an overall decrease in the assortativity of modules (Cao et al., 2014). Furthermore, studies using structural networks reported an increase in between-module connectivity when comparing two groups of younger and older adults (Chen et al., 2011). In (Baum et al., 2017) brain networks were analyzed in a restricted age range of 8–22 years, and a reinforcement of the hub edges between and within modules was demonstrated, associated with network maturation.

To date, two main strategies have been employed to track variations in the network architecture across stages of life: (i) comparison among representative networks or (ii) among averages formed over large groups. However, these strategies could be confounded by differences in network properties (Fornito et al., 2013; van Wijk et al., 2010) that are not of interest to the current analysis. In fact, topological measures, such as communities, depend on the network's density and edge distribution (Rubinov and Sporns, 2010), which vary not only across the lifespan (Betzel et al., 2014; Lim et al., 2015; Zuo et al., 2017), but also exhibit non-age related individual differences, making a comparison based on representative subjects difficult. At the same time, averaging networks across larger populations likely leads to significant loss of information.

In this work, we aim to investigate how the connectome's modular structure evolves during a large part of the lifespan, while addressing these methodological issues. We leverage an extensive neuroimaging dataset (620 subjects ranging from 7 to 85 years old), and we propose a novel framework, based on multilayer networks (De Domenico, 2017; Kivelä et al., 2014; Muldoon and Bassett, 2016; Vaiana and Muldoon, 2018) where layers represent narrow age ranges. The multi-layer model synthesizes connectivity information from multiple subjects, representing these data in a single network model without discarding data from any of the participants. Using this methodology, the variability of connection patterns across layers will be explicitly associated with age and, as a consequence, so will modular structure. Constructing ensembles of multi-layer networks, we systematically track the evolution of modular structure across the life span. Consistent with previous studies, we find an age-related loss of connectivity within modules. Our study adds to our current understanding of age-related changes in the organization of the connectome, specifically its modular organization. Moreover, our ensemble multi-layer network approach may be useful for future statistically robust investigations of network topology across large imaging or biomedical datasets.

2. Methods

2.1. Experimental dataset and data processing

The main objective of this work is to study how the modular organization of the brain connectome evolves during the lifespan. For this purpose, we leveraged the openly available Nathan Kline Institute – Rockland Sample dataset (NKI-RS, http://fcon_1000.projects.nitrc.org/indi/enhanced/); an ongoing project which aims to collect a large scale ($N > 1000$) community sample of participants across the lifespan (Nooner et al., 2012). Institutional Review Board approval was obtained for this project at the Nathan Kline Institute (#226781 and #239708) and at Montclair State University (#000983 A and #000983B) in accordance with relevant guidelines. All participants gave written informed consent or assent. The anonymized dataset is freely available through an Amazon S3 Bucket at http://fcon_1000.projects.nitrc.org/indi/enhanced/neurodata.html. Both T1-weighted (T1w) and diffusion (dMRI) images are provided, collected with a 3T Siemens Magneton Tim Trio scanner, using a 12-channel head coil. T1w images were pre-processed with the *FreeSurfer* (http://surfer.nmr.mgh.harvard.edu/) *recon-all* pipeline to reconstruct the *Yeo17* network parcellation, which renders 114 cortical nodes (https://github.com/ThomasYeoLab). dMRI images were denoised, corrected for motion and susceptibility distortion, and then aligned to the corresponding T1w. Deterministic streamline tractography was run using *Dipy* (Garyfallidis et al., 2014). Finally, we extracted the structural connectivity matrices normalizing the number of streamlines that connect each region of interest (ROI) of the network parcellation, by the geometric mean volume of the connected ROIs (regions of interest) (Betzel and Bassett, 2018; Faskowitz et al., 2018). In this way, we obtained weighted anatomical connectivity matrices where weights represent the connection density between brain regions. We performed rigorous quality control on these matrices excluding subjects based on T1w viability, presence of artifacts on dMRI, quality of tractography reconstruction and excessive sparseness of the adjacency matrix. More details about data processing can be found in (Faskowitz et al., 2018).

2.2. Multilayer networks construction

Following data processing, we obtained an ensemble of 620 anatomical weighted networks covering participants non-uniformly distributed between 7 and 85 years old. The networks were summarized as adjacency matrices $\boldsymbol{W} = [w_{ij}]$, made of $N = 114$ nodes representing cortical ROIs of the Yeo parcellation (Thomas Yeo et al., 2011), $ij \in [1,\ 114]$, whose entries denote the structural connection weights between each pair of nodes.

From these data we constructed a multilayer network in which layers represent sequential and heterogeneous age groups of people. We implemented a statistical method based on bootstrap theory (Efron and Tibshirani, 1993) which is summarized in Fig. 1. This procedure included:

a) dividing the entire dataset into 2-year temporal bins, i.e. $NG = 39$ groups of subjects equally spaced in time, each one spanning 2 years;
b) assigning subject-level network to every single bin.

Since in (a) the number of the participants was not uniformly distributed across the groups, we obtain the networks in (b) through a reiterated probabilistic procedure based on two phases:

b. i) bootstrapping with replacement: we randomly picked 10 networks within each temporal bin;
b. ii) averaging of these networks to obtain one for each bin.

In order to avoid an artificial increase in network density, we employed an averaging process that maintains the mean number of connections over the 10 networks, by removing extra edges. In doing so, we take into account that anatomical brain networks usually have strong short-distance and weak long-distance weights (Betzel et al., 2018a; Betzel and Bassett, 2018). Thus, simply removing the weakest edges after averaging would lead to networks with only short-distance connections, which is not realistic. Rather, we evaluate the frequency with which

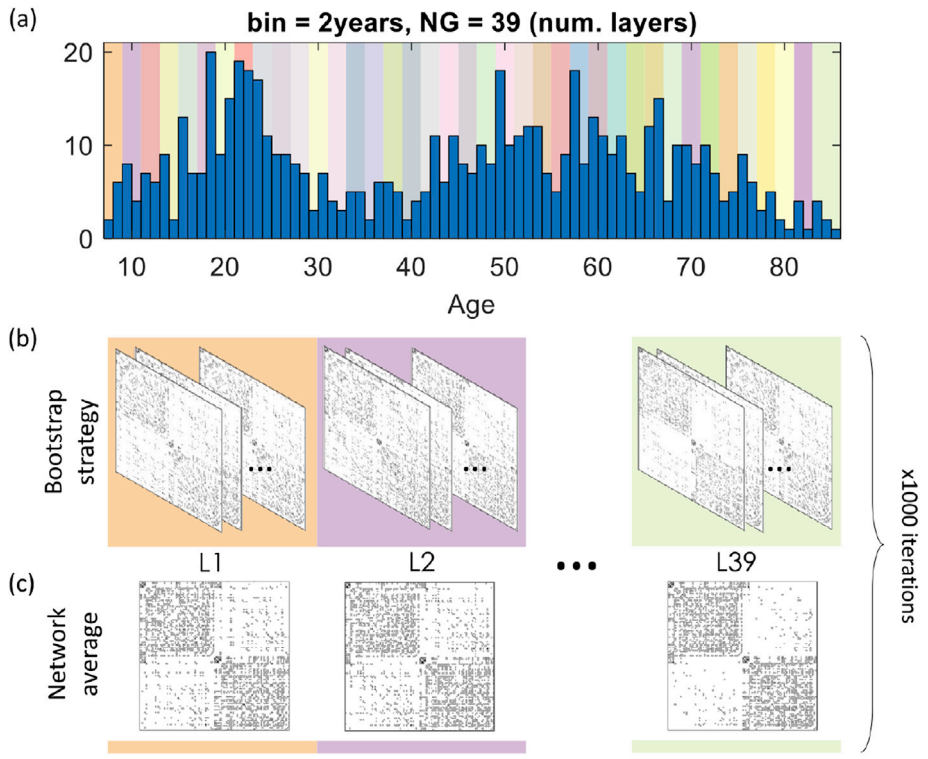

Fig. 1. Schematic representation of the steps undertaken to obtain the multilayer network. Panel (a): division of the dataset into 39 temporal bins, identified by color code, each spanning 2 years and comprised of a different number of subjects. Panel (b): random selection of 10 networks within each temporal bin. Panel (c): averaging of each subset of networks. The procedure in panels b and c is iterated 1000 times to obtain 1000 multilayer networks made of 39 layers.

connections occur, and we remove edges starting from the least frequent, until we obtain a network whose density is equal to the mean density computed over the 10 networks. In a way similar to (Betzel et al., 2018a), we preserve the edge length distribution. Finally, we repeat steps (b.i) and (b.ii) many times (nIT = 1000) to obtain an ensemble of equivalent multilayer networks made of NG layers representative of the lifespan human connectome at NG consecutive age stages.

2.3. Multilayer and multiscale community detection

The primary focus of this work is on brain network organization from the modular structure point of view. To recover the modular organization of the inferred networks we adopted a multilayer community detection algorithm. Numerous previous studies have used modularity maximization (achieved through optimizing a modularity quality metric, Q) for uncovering the modular structure of brain networks (Sporns and Betzel, 2016). Modularity (Q) (Girvan and Newman, 2002; Newman and Girvan, 2004) assesses the goodness of a given partition with respect to a null model so that the maximization of Q returns a plausible partition of the network into non-overlapping modules. Here, we employed a multilayer version of the modularity quality function (Mucha et al., 2010) which has the following form:

$$Q_{ml} = \frac{1}{2\mu}\sum_{ijrs}\left\{\left(A_{ijr} - \gamma_r P_{ijr}\right)\delta_{lr} + \delta_{ij}\omega_{jrs}\right\}\delta\left(g_{ir}, g_{js}\right) \quad (1)$$

With:

- i,j network nodes;
- r,s network layers;
- 2μ total weights of the edges;
- A_{ijr} weight of the edge linking nodes i and j in layer r;
- γ_r spatial resolution parameter;
- P_{ijr} weight of the edge linking nodes i and j in layer r in the null model;
- ω_{jlr} temporal resolution parameter;
- $\delta_{lr} = 1$ if r=s, and 0 otherwise;
- $\delta_{ij} = 1$ if i=j, and 0 otherwise;
- g_{ir} cluster to which node i is assigned at layer r;
- $\delta(g_{ir}, g_{js}) = 1$ if $g_{ir} = g_{js}$, and 0 otherwise.

Though there exist many possible null model definitions, the most common (and the one used here), is the configuration model $P_{ij} = \frac{k_i k_j}{2m}$, in which each node's connection strength is preserved but edges are placed in a random fashion. The optimization of the multilayer modularity can be used to identify assortative communities at different scales by varying its spatial and temporal resolution parameters, γ and ω. The value assigned to the spatial resolution parameter γ influences the number and size of the detected modules. When γ is small many elements A_{ijr} will probably exceed the null model, and consequently, maximizing Q_{ml} would produce few large communities. Vice versa, high γ-values are likely to produce many small communities. The temporal resolution parameter, ω, corresponds to the strength of the edges linking a node to itself across layers. Formally, these links can be placed in an all-to-all configuration (nodes are connected to their counterparts across all layers of the network) or in a temporal configuration (nodes are connected only across consecutive layers of the network). We adopted the secondway of representing inter-layer connections, conceptualizing the multilayer network as a temporal network (Holme, 2015; Holme and Saramäki, 2012). It is reasonable to think that the healthy brain network architecture varies continuously according to a temporal model, in which the structure re-organizes continually year to year (i.e. layer by layer). The value of ω impacts the homogeneity of the community assignments across the layers. Intuitively, when ω = 0 nodes are uncoupled across layers and maximizing Q_{ml} would be akin to maximizing Q separately in each layer. More generally, small and large ω-values lead to variable and stable partitions, respectively. A multilayer approach, with ω > 0, is well suited for a lifespan study. A reasonable expectation is that the networks and their partitions derived from consecutive layers (e.g. 29–30 and

31–32 years old) share significant overlap and resemble each other. Because the connectome's modular structure spans multiple scales, all potentially plausible (Betzel and Bassett, 2017), we considered partitions obtained with different combinations of resolution parameters, $\gamma = [0.5, 1, 2]$ and $\omega = [0.1, 0.5, 1, 5]$, in order to obtain modules diversely resolved in the cortex and across ages. We optimized multilayer modularity using the free *genlouvain* package implemented in MATLAB (Jutla et al., n.d.), which consists of a generalized version of the Louvain algorithm (Blondel et al., 2008).

2.4. Analysis of the communities

Through the multilayer modularity maximization, we obtain an ensemble of multilayer partitions – 1000 per each combination of γ and ω – that we characterized by computing several measurements.

2.4.1. Statistics of multilayer modularity maximization

First, we derived the Variation of Information (VI) matrix. This is a measure of distance between two partitions (Meilă, 2007), closely related to the mutual information and entropy of the communities. Each entry *rs* of the VI matrix corresponds to the VI value computed between the partitions at layers *r* and *s*. We compute the VI matrix for each combination of the resolution parameters in order to identify interesting community structures and exclude non-interesting ones for the aim of our study. In fact, even if multiple partitions of the connectome at different temporal scales are plausible, we focus on those that show a reasonable variation over the lifespan. Therefore, we omit partitions relative to ω values producing communities that do not consistently vary across the layers, or whose variation rate is excessively high even over networks representing close ages. By calculating the distance between each pair of partitions we can evaluate the magnitude of variations across the layers.

We also restrict our investigation to a specific spatial scale. We wanted to analyze partitions with a number of clusters consistent with the number of large-scale anatomical or functional subnetworks derived in previous work (around ten) (Eickhoff et al., 2007; Thomas Yeo et al., 2011). Thus, we computed the number of clusters and their dimension and we excluded those γ-values that returned partitions with too few clusters. Among the parameter values we considered for γ and ω we identified a combination that returns a multilayer community structure C_{opt} with a biologically plausible number of modules that exhibit a reasonable rate of reconfiguration on a physiological time scale. The following metrics focus on this subset of communities.

2.4.2. Age-related changes of the modular structure

For every partition of C_{opt}, we computed the single layer modularity, whose expression is reported in Eq. (2):

$$Q = \frac{1}{2m_r}\sum_{ij}\left[\left(A_{ijr} - \gamma_r P_{ijr}\right)\right]\delta\left(g_{ir}, g_{jr}\right) \tag{2}$$

With:

- $2m_r = \sum_{ij} A_{ijr}$;

We then evaluated the node and layer flexibility (Bassett et al., 2011b). We built a flexibility matrix *F* of dimension $[N*(NG-1)]$ and filled its columns either with ones or zeros depending on whether node *i* has changed cluster assignment going from layer *r* to layer $r + s$ or not. The average over the rows and columns will return the node and the layer flexibility, respectively. The node flexibility, f_i, represents the percentage of partitions in which node *i* changes its community allegiance. It allows us to quantify the strength with which brain regions reconfigure across the lifespan. The layer flexibility, f_l, is measured between all the pairs of consecutive partitions and captures the average node flexibility between such partitions: $f_{l(rs)} = \frac{1}{N}\sum_i f_{irs}$. It enables us to investigate the possible existence of age stages in which brain modular organization strongly rearranges.

Then, we examined how the distribution of the modules on the cortex varies with age, tracking their disposition within and between the hemispheres.

Finally, for each node and for each layer we calculated the participation coefficient (Guimerà and Amaral, 2005), (Eq. (3)):

$$p_i = 1 - \sum_c \left(\frac{k_{ic}}{k_c}\right)^2 \tag{3}$$

With:

- k_{ic}: total weights involving node *i* within module *c*;
- k_c: total weights inside cluster *c*.

This measure captures how the connections of node *i* are distributed across all the modules. By computing p_i across the lifespan, we aim to reveal if the brain's sub-systems become more segregated or integrated during specific time periods.

The above-listed measures were computed on each one of the 1000 resulting multilayer partitions. We verified the significance of the temporal evolution of these measures through a comparison with a temporal null model in which time is scrambled by randomly permuting the network's layers. This kind of null model has been proven particularly useful in the study of the temporal multilayer networks, in theoretical works investigating the evolution of the properties of temporal networks (Pan and Saramäki, 2011; Starnini et al., 2012), in application in social networks (Backlund et al., 2014; Cardillo et al., 2014), as well as in the study of brain networks mesoscale organization (Bassett et al., 2013, 2011b). We built an ensemble of null-case multilayer networks following steps a) and b) of section 2.2 and then randomly permuted the network's layers within each iteration. The use of such a null model allowed to test whether results obtained from the ensemble of lifespan multi-layer networks were robust against permutations of the age structure of the data. Thus, within each time point, we statistically compared the distribution of the values of the indices computed on the actual model with those computed in the null model. We made this statistical comparison through a permutation test, with 100.000 permutations and a significance $\alpha = 0.05$. We could perform this temporal validation thanks to the 1000 replications that we had available for both models, which resulted in two different distributions of the communities-related indices (for each layer).

3. Results

The principal aim of this study was to investigate age-related changes of the human connectome modular organization. For this purpose, we processed diffusion MRI data of the NKI dataset and implemented a probabilistic procedure to obtain an ensemble of multilayer networks representative of the anatomical connectome at different ages. Each layer represents a mean model of structural connectivity in an age range covering 2 years. Since the participants ranged from 7 to 85 years old, we obtained multilayer networks constituted by 39 age-dependent layers (Fig. 1). We generated an ensemble of 1000 such multilayer networks, and we identified their modular structure through a multilayer modularity optimization algorithm, obtaining for each layer the brain regions' community assignment. The output of this algorithm depends on two parameters defining spatial and temporal resolution, γ and ω. We tuned both parameters in order to examine partitions at different spatial and temporal scales, which affect the number of clusters, their size, and their reconfiguration rate across the lifespan.

3.1. Statistics of the multilayer multiscale modularity maximization

First, we quantified the extent to which brain regions reconfigure

across age as a function of the temporal resolution parameter, which plays a key role in this regard. We report in Fig. 2 the VI matrices obtained for each tested parameter combination. VI matrices are square matrices of dimensions equal to the number of layers (i.e. 39), in which each entry represents the distance between layer *r* and layer *s*. They allow us to visually evaluate the similarity of partitions across layers. As expected, running the multilayer modularity optimization with low ω-values produces communities that rarely cover multiple layers, and the dissimilarity score between two general partitions *r* and *s* is high. In contrast, increasing ω-values yields stable communities that span several layers, and the VI between two partitions *r* and *s* is low. All the temporal scales defined by the different ω-values could be of interest. For example, stable partitions across the layers, produced with high ω, could highlight possible structures that do not change over the lifespan. On the other extreme, highly age-specific partitions, produced through low ω, could represent community structure expressed in specific age ranges. Here, we are interested in an intermediate regime, in which modules reconfigure across longer time periods, while also remaining robust across shorter time periods. Hence, we adopted $\omega = 0.5$. Here, communities tend to be similar along the main diagonal of the matrix (VI $\approx$ 0), namely along consecutive years of the lifespan, but they diverge more and more farther away from the main diagonal. In contrast, with lower ($\omega = 0.1$) and higher ($\omega = [1, 5]$) values of inter-layer coupling, partitions respectively appear highly variable, even between consecutive layers, or barely variable, even at the extremes of the lifespan.

Second, we examined how cluster numbers and their sizes vary among different γ-values, in order to identify a spatial scale in which the number of modules is congruent with the number of subnetworks encountered in previous studies (Eickhoff et al., 2007; Thomas Yeo et al., 2011). Going from low to high γ-values we pass from a coarser to a finer scale (Fig. 3). On average, setting $\gamma = 0.5$ yielded 2–3 modules comprising about 40–60 nodes each. By increasing γ to 1 we obtained partitions made of 4–6 modules composed of 20–30 nodes. Finally, with $\gamma = 2$ we found on average 9–12 clusters made of 8–12 nodes each, for a partitioning scheme that most closely resembles the number of large-scale anatomical and functional systems derived in previous studies (Eickhoff et al., 2007; Thomas Yeo et al., 2011). Different γ-values also affect how clusters rearrange across the lifespan (Fig. 3, panel *c*). We found that for $\gamma \leq 1$ the number of communities decreases with age, going from 3 to 2 ($\gamma = 0.5$ green subspace) and from 6 to 4 ($\gamma = 1$, yellow subspace), while for $\gamma = 2$ this number increases from 9, in the early lifespan, to 12, in the late lifespan (violet subspace). Among the three values of γ, only $\gamma = 2$ produces continuous variations in cluster sizes. This setting not only seems to be more physiologically interesting, but also better matches our model, which is designed to track modules' evolution over multiple narrow adjacent temporal bins, and not over big age ranges.

Given these considerations, we restrict the following investigations on the multilayer modular structure identified by optimizing the multilayer modularity in the subset of parameters [$\gamma = 2$, $\omega = 0.5$]. By selecting a number of clusters around 8–12 allows us to relate them to previously established subdivisions of the brain into functionally specialized systems. Lower γ-values produce partitions with only few clusters which can be trivially reduced to the two hemispheres, while higher values of γ

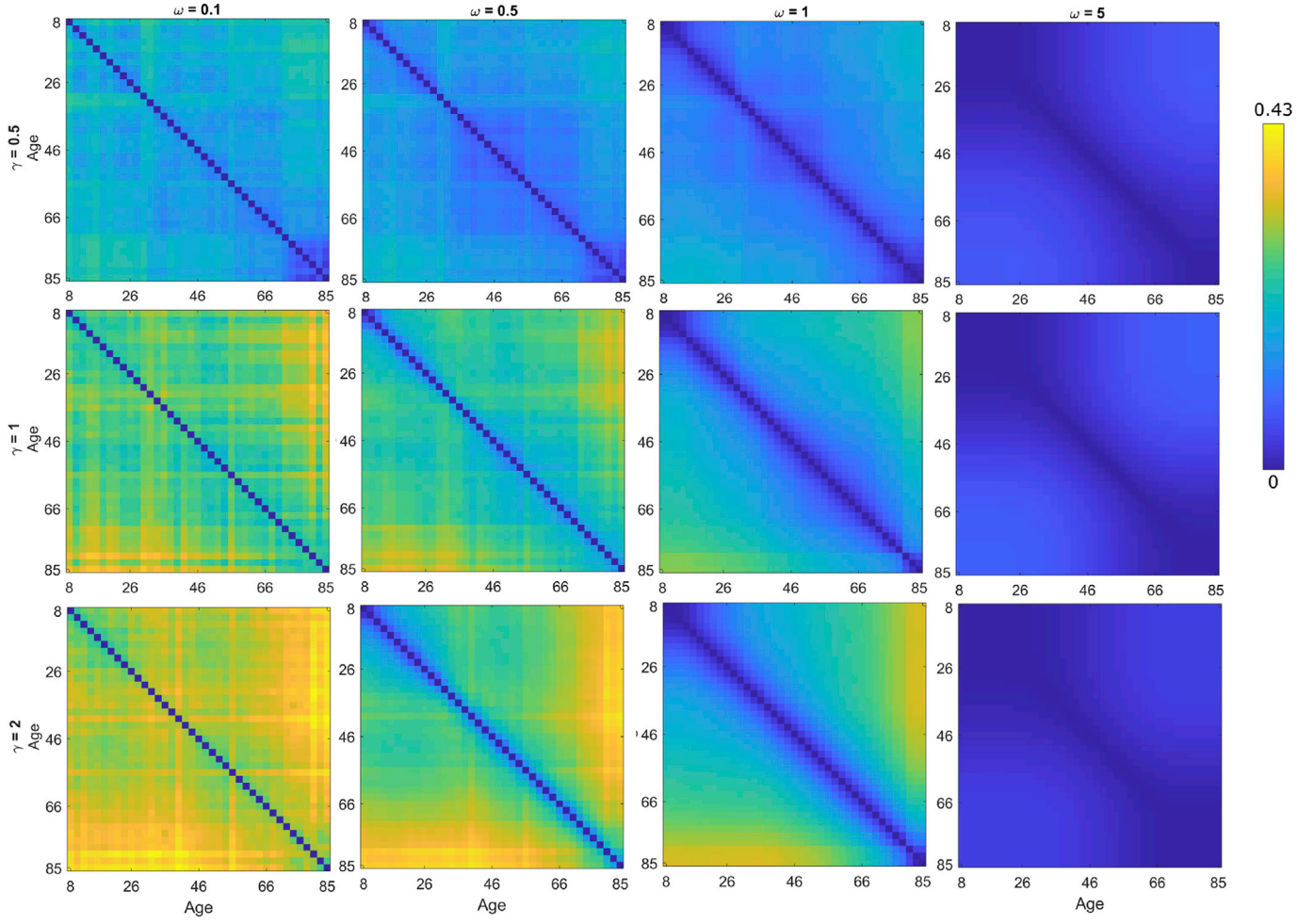

Fig. 2. Variation of Information (VI) matrices computed for each combination of γ and ω (reported in rows and columns). In each matrix, entries represent the VI computed between two layers r and s. Values span the range [0, 0.43].

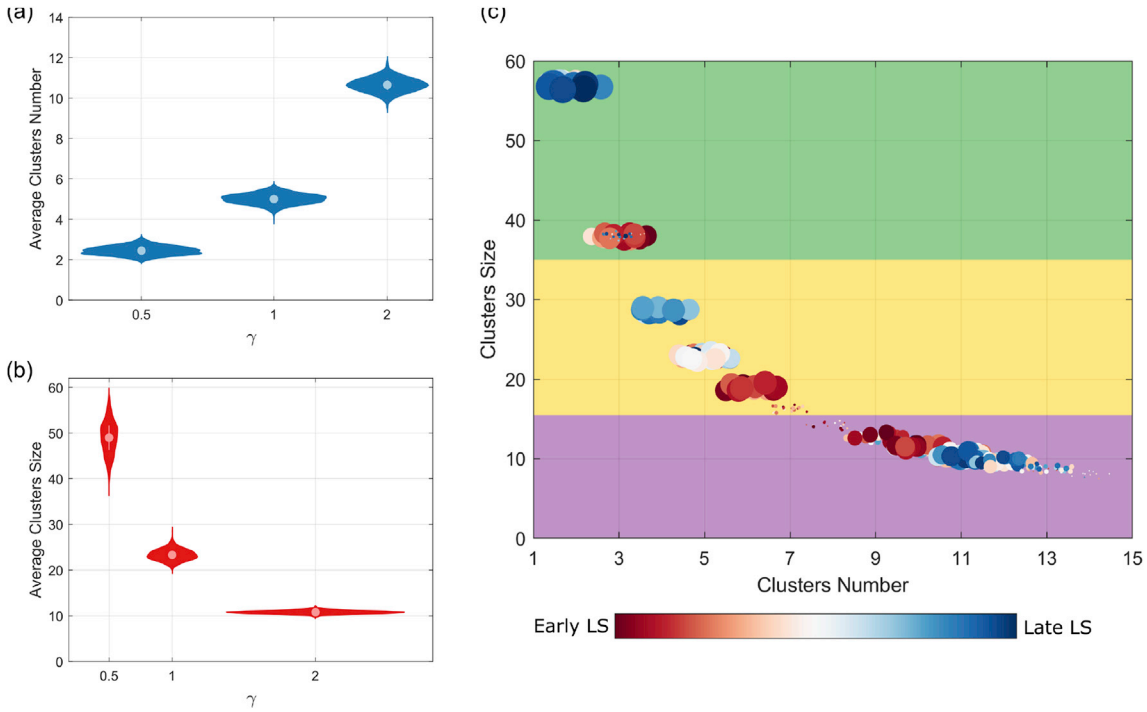

Fig. 3. Clusters number and clusters size of the partitions detected with ω = 0.5. Violins in panels (a–b) report their average distribution over the 39 layers and 1000 iterations, for each γ value. Panel (c) shows how clusters number (x-axis) and clusters size (y-axis) vary as a function of age and γ. Age is indicated with colors, from red (early lifespan) to blue (late lifespan). The dimension of the dots in the scatterplot is proportional to the frequency with which that value is observed across the 1000 multilayer networks. We render a scatterplot for each γ value [0.5, 1, 2], which occupy the xy plan in three different zones (green, yellow and violet).

would lead to larger numbers of communities composed of few nodes, which do not match with established schemes for functional systems in the human brain.

3.2. Age-related changes of the modular structure

First, we aimed to find any relationship between age and segregation of the brain subnetworks. For this purpose, we computed on each layer separately the single layer modularity Q (Eq. (2)). Modularity returns an estimation of the extent to which communities are internally connected or segregated one from another. We computed Q both for our actual model (Q_{obs}) and for the null model (Q_{null}). We found (Fig. 4) that Q_{obs} varies systematically with age, following a U-shape, while Q_{null}, does not show any age-related trend. In the early (7–20 years) and in the late (72–85 years) lifespan, Q_{obs} is statistically higher than Q_{null}. In contrast, in the middle lifespan (20–72 years) Q_{obs} shows lower values than Q_{null}.

In order to explain this trend, we calculated the number of intra-cluster edges (example in Fig. 4, panel *c*) and their weights across the layers of the network. Indeed, given a network and a partition of its nodes into modules, Q is proportional to the difference between the within-module weights of the network and those in the configuration null model multiplied by γ, within each cluster (Eq. (2)). The results (Fig. 4, panel *b*) suggest that there are two factors contributing to increased modularity observed at the extremes of lifespan. As for the early lifespan, the number of intra-clusters edges is considerably higher than in the following middle lifespan (a validation of this trend is proposed in the Supplementary Information, section S3). This number and age are negatively correlated (*p-value* < 0.0001, $r = -0.58$), suggesting that aging is associated with a loss of intra-clusters edges, probably causing higher modularity values in this first part of the considered timeline. In the late lifespan, instead, the weights of the intra-clusters' edges are significantly higher. This variable positively correlates with age (*p-value* < 0.0001, $r = 0.72$), resulting in higher modularity at the end of the age range. To further demonstrate these two factors driving modularity, we plot the Q_{obs}-values with respect to the intra-clusters' weights and edges (Fig. 4, panels *d-g*), exhibiting a positive and negative tendency, respectively. Thus, weather Q_{obs} increases or decreases with age is an effect of the edges' distribution within clusters, their weights, and their relationship with the configuration null model.

Next, we quantified the extent to which modular structure changes with age, and which brain regions are more likely to change community membership, by analyzing the layer and node flexibility, F_l and F_i (Fig. 5), comparing observed and null models. The layer flexibility of our model, $F_{l\text{-}obs}$, resulted in values in the range [0.02, 0.2] (Fig. 5, panel *a*). It shows high dependency with age as it monotonically increases across the temporal bins (computing the Spearman correlation between $F_{l\text{-}obs}$ and age was significant ($r = 0.76$, *p-value* <0.0001)). This suggests that among older participants, modules reconfigure more compared to younger participants. Conversely, no age-related trends were found in the null model, $F_{l\text{-}null}$, whose values remain around an intermediate level, ~0.14, across the entire lifespan. In the first part of the lifespan, until 36 years old, $F_{l\text{-}obs}$ is lower than $F_{l\text{-}null}$, while in the late lifespan, from 72 years old, it becomes significantly higher. In the middle part of the lifespan, $F_{l\text{-}obs}$ and $F_{l\text{-}null}$ assume similar values.

Looking into node flexibilities, we determined which brain regions are more prone to change modular allegiance (Fig. 5, panel *b*). Overall, the medial part of the cortex surface is less flexible with respect to the lateral one. The less flexible brain nodes belong to the visual cortex and the auditory area. On the contrary, the temporal lobe, Wernicke's area, and the pre-frontal lateral cortex have higher F_i values. These regions are functionally involved in the posterior dorsal attention subnetwork, the temporo-parietal default mode network (DMN), and the limbic area (Fig. 5, panel *c*). We also examined F_i within specific age ranges, 7–38 and 38–85 years old (Fig. 5, panels *d-f*), as in these periods the F_l exhibits different trends in the actual and the null model. Generally, brain areas more flexible in the early lifespan remain more flexible in the late lifespan. The only exception is represented by nodes located in the inferior temporal cortex, which change from lower to higher flexibility across age.

We then examined how structural modules are topographically

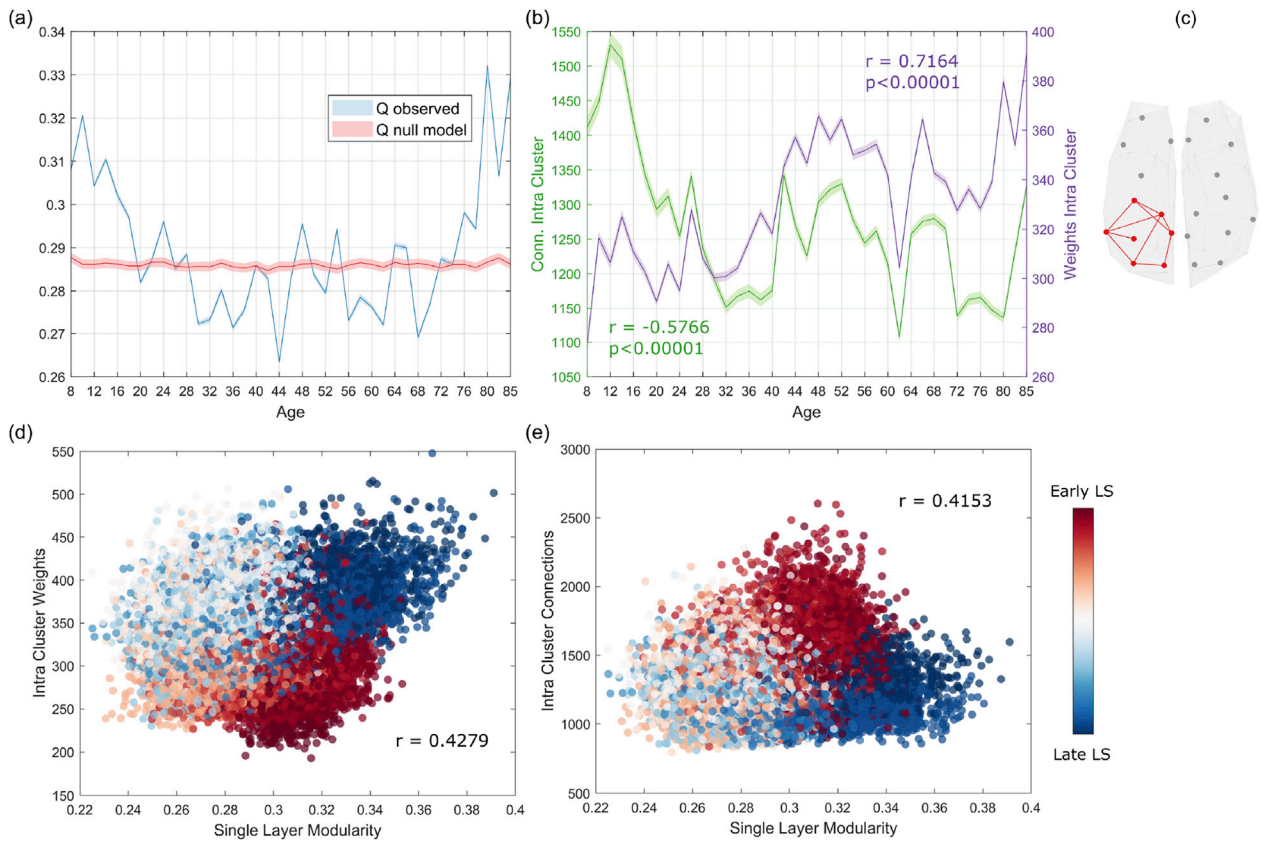

Fig. 4. Single-layer modularity. Panel (a): trend of the modularity across the layers for the actual model (blue) and the null model (red). Panel (b): trend of the number (green) and weights (violet) of intra-clusters connections. In both panels bounded lines represent the mean and confidence interval over the 1000 iterations. Panel (c): example of a cluster with its intra-cluster links. Panels (d–e): scatter plot and 2D histogram of the weights of intra-clusters edges against single layer modularity (for all the 1000 multilayer networks). Dots are colored according to age, from dark red (early lifespan) to dark blue (late lifespan). We also report the mean Pearson correlation coefficient computed between the two variables (calculated considered only the significant outputs ($p < 0.05$)). Panels (f–g): scatter plot and 2D histogram of the intra-clusters' connections.

distributed on the cortical surface across the lifespan. In Fig. 6, panel *a*, we display for each temporal bin the number of clusters that span both hemispheres. While in the null model this number does not change across layers, with the intact model it is first higher and then diminishes. Until the middle lifespan there are 6 clusters involving brain areas of both hemispheres. Given that in this portion of the lifespan we counted 9 to 10 clusters, this means that most of them involve both the right and left hemispheres. After the middle lifespan the number of modules spanning the two hemispheres linearly decreases with age until, in the last temporal bin, only one cluster exhibits this feature, essentially comprising brain areas located on the anteromedial cortex, and partially in the medial sensory association area (Fig. 6, panel *f*).

To understand a plausible cause for this drop of inter-hemispheric modules, we examined how the number of edges and their weights are dispersed within and between the hemispheres during the lifespan (Fig. 6, panels *b-c*). While the amount of intra-hemispheric connections is constant, inter-hemispheric connections decrease. Interestingly, this decrease starts at the same period in the lifespan where the number of inter-hemispheric clusters begins diminishing, ~48 years old. Observing the weights of the connections, this consideration is even more accentuated, as the inter-hemispheric weights drop, and the intra-hemispheric ones increase. Thus, the age-dependent loss of inter-hemispheric connections appears associated with a reconfiguration of structural modules to become hemispheric-specific. Indeed, inter-hemispheric weights and number of hemispheric specific modules were found to be highly correlated ($r = 0.89$, *p-value* < 0.0001) (Fig. 6, panel *d*).

Finally, we wanted to characterize the integration of the different brain areas with respect to the whole network and the modules to which they belong. We did so computing for each node the participation coefficient p_i, as it quantifies how uniformly distributed its connections are across modules. The smaller it is the more the node interacts exclusively with other nodes of the cluster to which it belongs. We report the participation coefficient values of each layer, $p_l = \frac{\sum_i p_i}{N}$, across the ages, for the actual ($p_{l\text{-}obs}$) and the null ($p_{l\text{-}null}$) models (Fig. 7). The $p_{l\text{-}null}$ values do not show any age-related trend, remaining around 0.61, while $p_{l\text{-}obs}$ exhibits an inverted U-shape trend. Its values increase in the first part of the lifespan, until ~32 years old, going from 0.56 to 0.62. Then, it remains in the range [0.6, 0.63] until ~ 72 years old, to finally decrease until the last layer, reaching a value of 0.57. This trend confirms that early and late lifespan are characterized by well-segregated sub-systems, while in the middle lifespan brain regions interact more closely despite their membership in system-specific modules. To explain this trend in $p_{l\text{-}obs}$, we looked at the number of the inter-cluster edges over the years (Fig. 7, panel *b*), discovering that they also follow an inverted U-shaped curve.

We identified brain nodes that mostly contribute to this non-linear trend, by finding those whose integration in the network is significantly influenced by age. For each node, we computed the Spearman correlation between p_i and age in three different ranges: 7–38 years old, 38–85 years old, 7–85 years old. Within the first age range, almost all the brain regions' p_i are positively correlated with age; nodes belonging to the somatosensory and sensory association areas both in the medial and lateral parts of the cortex are those mostly contributing to this trend. Such regions subtend the control, limbic and DMN networks. During the second interval, most of the nodes' p_i are negatively correlated with age. Specifically, somatosensory association areas and dorsal attention areas

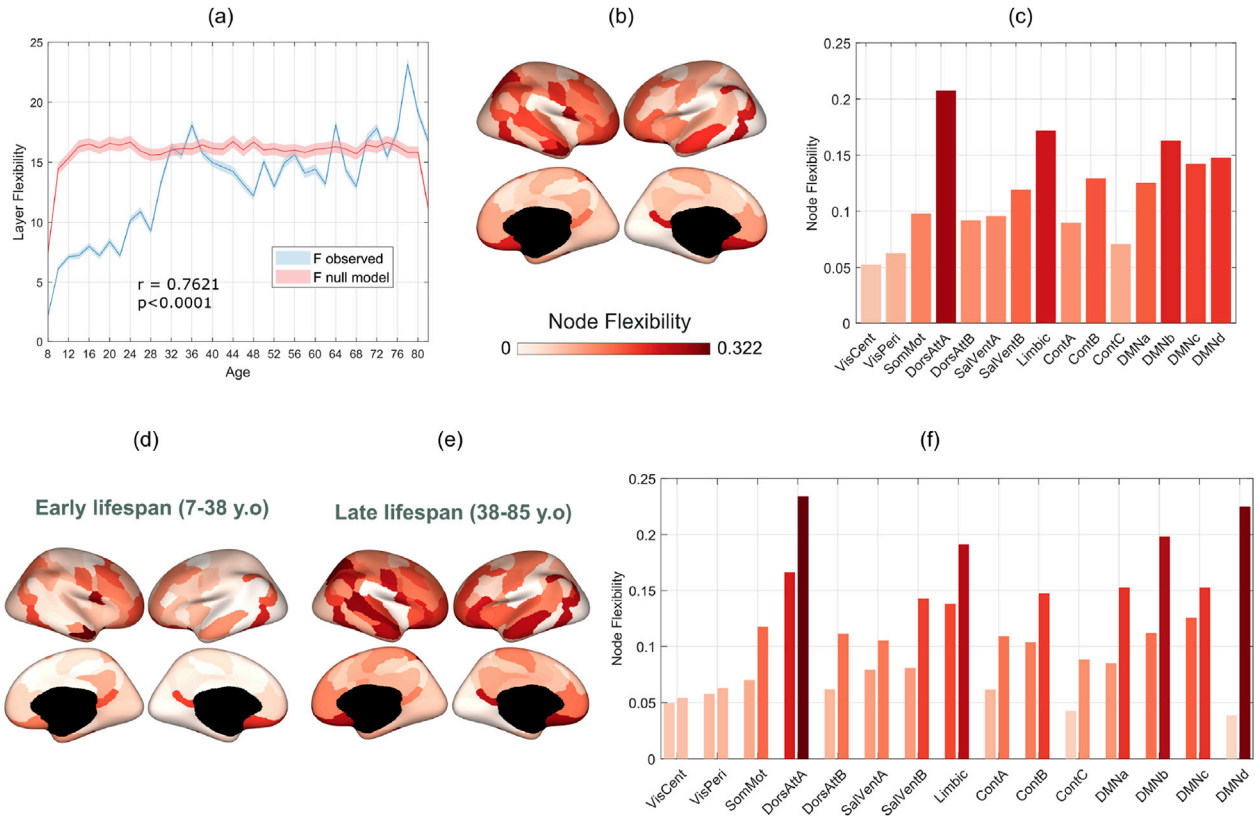

Fig. 5. Flexibility. Panel (a): trend of the layer flexibility across the lifespan for the actual model (blue) and the null model (red). The bounded lines represent mean and confidence interval computed on the partitions of the 1000 equivalent multilayer networks. Panel (b): mean nodes flexibility across the lifespan (averaged over the 1000 iterations). Brain regions are colored from white to dark red proportionally to their flexibility value. Panel (c): Nodes flexibility averaged within the functional subsystems of the current parcellation. Panels (d–f): nodes flexibility and their average within the functional subsystems in the age ranges [7, 38] and [38, 85] years old. Left (right) bars in panel (f) are referred to younger (older) participants.

as well as the medial visual cortex and the pre-frontal cortex associated with the medial DMN become strongly anti-correlated with age. In contrast, the temporal cortex (the areas subtending the control network and the temporal DMN) instead, remains positively age-correlated. Looking at the entire lifespan, we identified two sets of nodes whose p_i significantly correlates with age in a positive and negative direction respectively. The temporal cortex and sensory areas fall in the first case, while the prefrontal cortex and somatosensory association brain regions in the second one. Overall, the visual cortex and the medial DMN are systems whose integration with the network is less affected by age.

4. Discussion

In this work, we address a number of open questions regarding the network structure of connectome across the lifespan by developing and applying a novel ensemble multi-layer approach. In doing so, we provide a plausible description of the evolution of the connectome's modular structure during a large portion of the lifespan.

4.1. Age-related description of the connectome's modular structure

The results obtained in this study confirm that the human connectome's modular structure is age-dependent. Our first finding saw the number of clusters increasing with age, from 9 in the early lifespan to 12 in the late lifespan, while, as a consequence, their size decreases. The metric of modularity exhibits an age-related U-shaped trend (Fig. 4), with higher values at the beginning and at the end of the age range. Nonlinear U-shaped trends, with opposite trends over the early and the late lifespan, are often encountered in lifespan studies, prompting a fundamental question about the relationship between patterns of brain connectivity during development and aging: is the aging process a simple reversal of the developmental one? Or does the U-shape arise as a result of distinct processes? We tried to answer these questions by looking at the number and weight of intra-modules edges, which showed a decreasing and increasing trend, respectively. We found that high values of modularity may be due to two different processes: in the early lifespan modules are internally densely connected, while in the late lifespan they are internally strongly connected. These results agree with previous findings, where an overall decrease of cortical connectivity with age has been observed (Betzel et al., 2014; Dennis et al., 2013; Gong et al., 2009; Hagmann et al., 2010), linked in (Lim et al., 2015) to loss of within-module connectivity through preferential detachment. The same mechanisms, plus the inverted U-shaped trend observed for the number of inter-clusters connections, may contribute to form the non-linear (inverted U-shaped) curve followed by the participation coefficient (Fig. 7).

While modularity and participation coefficient exhibit non-linear age-dependent behavior, we found that the flexibility of brain regions linearly increases with age (Fig. 5), indicating that modular organization tends to reconfigure more and more as age advances. This result aligns with those in (Wu et al., 2012), where connectome's properties have been analyzed over three age stages (young, middle, and old), and differences in the modules composition have been observed only between the last and the first two groups, but not between the first two. Another variable that varies linearly with age, decreasing from the maturation to senescence, is the number of modules that span both hemispheres (Fig. 6). We demonstrated that this is due to a drop in inter-hemispheric connections, possibly caused by a physiological age-related shrinkage of the corpus callosum (Raz et al., 2010).

Some brain regions appeared to be less prone to age-related changes, such as the medial cortex, the anterior cingulate, the orbito-frontal and

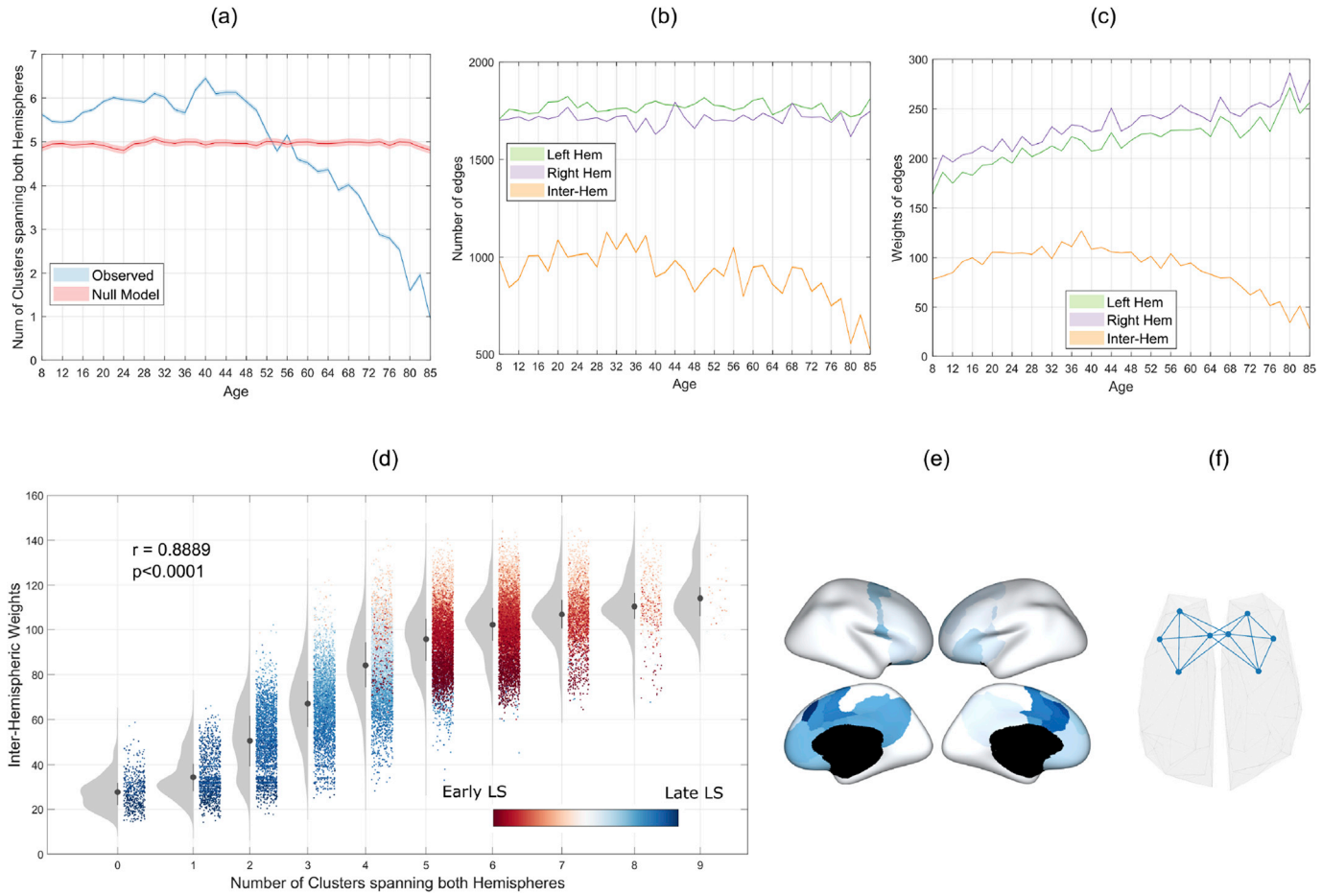

Fig. 6. Topographical clusters analysis. Panel (a): number of clusters that over the lifespan involve brain regions from both hemispheres, observed in our model (blue) and in the null model (red). Panel (b) and (c): trend across the lifespan of the number and weights of the connections located in the left hemisphere (green), right hemisphere (violet), and inter-hemispheres (orange). We report correlation coefficients and p-values of the Spearman correlation computed between the average of inter-hemispheric edges/weights and age. In all the three panels bounded lines indicate the mean and confidence interval of the distribution of such variables across the 1000 equivalent multilayer networks. Panel (d): rain-cloud plot of the inter-hemispheric edge weights against the number of clusters spanning both hemispheres. Dots are colored with an age-based criterion, from dark red (early lifespan) to dark blue (late lifespan). We also display the correlation coefficient and p-value of the Spearman correlation computed between the means of variables on the cartesian axis. Panel (e): Example of a cluster spanning the two hemispheres. Panel (f): heatmap on the cortex representing the brain regions that more frequently belong to the cluster that in the last temporal bin spans the two hemispheres. The blue intensity is proportional to this frequency.

superior-frontal cortex. They display low flexibility values, and their participation coefficient is not significantly correlated with age. Moreover, these regions constitute the cluster which continues spanning the two hemispheres into senescence. Interestingly, previous observations (Buckner, 2004) pointed out that changes in frontal-striatal circuits may be associated with a decline of memory and executive function. A previous study (Persson et al., 2006) suggested that older adults with declining memory performance show different DTI measures of the anterior white matter compared to older adults with intact memory functions. Also, the lateral occipital cortex shows low flexibility and non-age-related values of the participation coefficient.

The brain areas which reconfigure most across the lifespan are located mainly on the lateral part of the cortex, specifically in temporal regions, motor and sensory areas, the parietal lobe, and the posterior cingulate. Here we found high nodal flexibility, and a significant relationship between participation coefficient and age. However, these regions reconfigure in different ways. The participation coefficient of the temporal lobe and the superior central cortex subtending the sensory-motor area is positively correlated to age, so that these nodes become more integrated in the network with age. The opposite happens for the parietal cortex, whose participation coefficient is negatively correlated to age, becoming more segregated with age. These alterations we found on structural organization might underpin functional age-related alterations observed in the same areas in (Sambataro et al., 2010), where modifications of the DMN due to age have been associated to connectivity changes in the posterior cingulate cortex and the bilateral parietal regions, impacting the working memory functions, while no significative differences have been found in the anterior cingulate cortex.

We schematically summarize our findings reporting representative partitions (with lowest within-layer VI) at three age stages (Fig. 8). The network becomes more segregated with years, with the appearance of hemispherically-specific modules. The number of intra-cluster edges decreases with age, while their weight increases, causing non-linear trends of modularity and participation coefficient. Overall, the modules' reconfiguration rate increases with age.

4.2. *Methodological innovations of the multilayer framework*

Our study attempts to track multiple variables in a large, multi-modal dataset. Every approach used to detect changes in some variables must distinguish between meaningful trends and statistical noise. We tackled this challenge by implementing a probabilistic scheme, based on bootstrapping, that extracts an ensemble of multilayer networks, where layers represent homogeneous and contiguous age intervals. It also addresses a

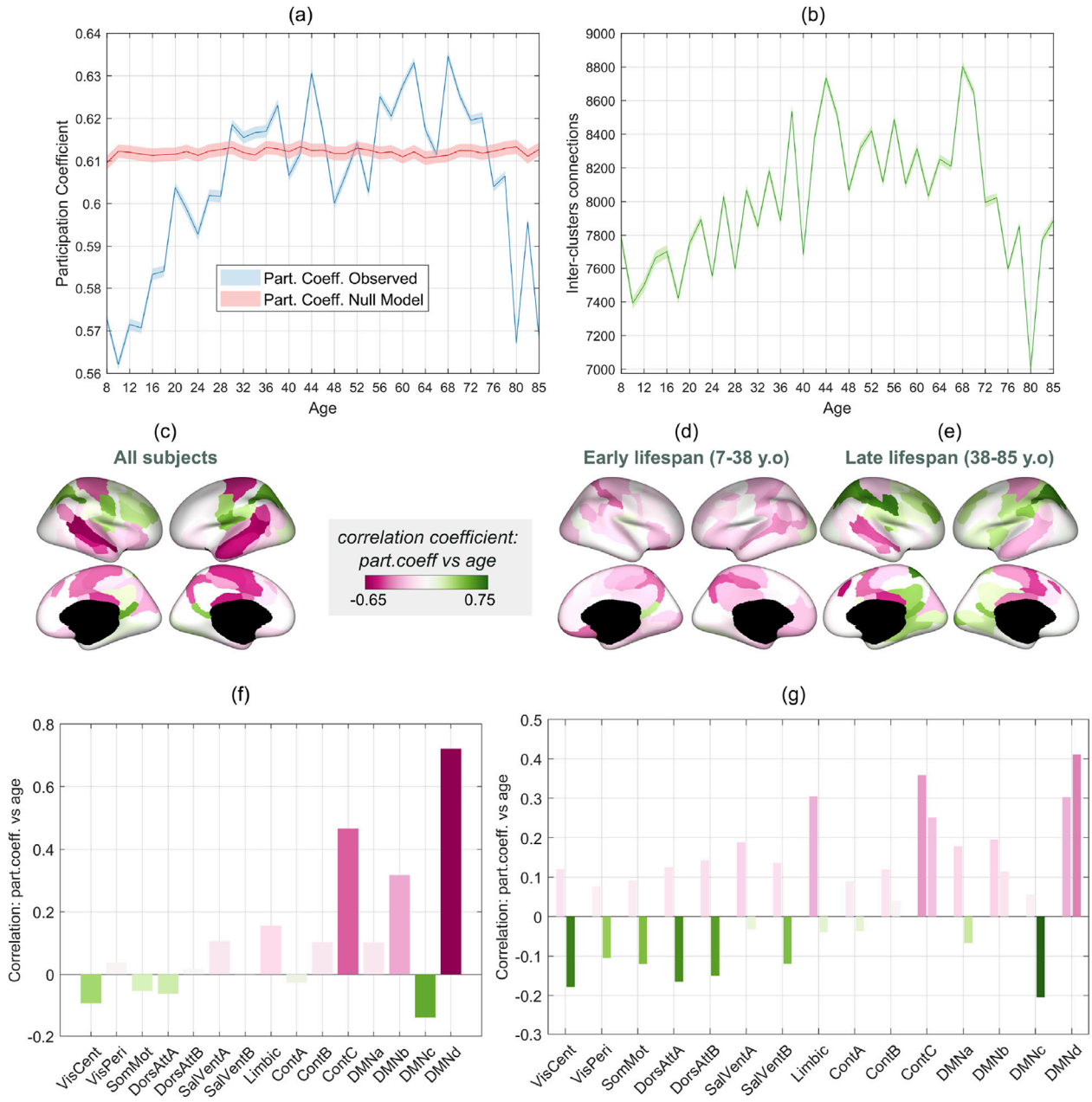

Fig. 7. Participation Coefficient. Panel (a): course across the lifespan of the participation coefficient (average among all the nodes) computed on the partitions of our model (blue lines) and the null model (red lines). Panel (b): trend of the number of inter-clusters connections. The bounded lines in panels a–b indicate the mean and confidence interval of the distributions of such variables over the 1000 iterations. Panel (c): representation on the cortex surface of the correlation coefficients of the Spearman correlation computed between ages and participation coefficient values of each node. Brain regions for which the outcome was not significant are white. Brain regions whose participation coefficient is significantly positively/negatively correlated with age are illustrated in pink/green. Panel (d): Average of the correlation coefficients within the functional subsystem identified by the current parcellation. Panels (e–g): representation on the cortex surface and average within the Yeo functional subnetworks of the correlation coefficients of the Pearson correlation computed between participation coefficient values and age in the range [7, 38] and [38, 85] years old. Left (right) bars in panel (g) are referred to younger (older) participants.

relevant issue in the context of comparison among subjects, or categories of subjects, based on the analysis of their MRI networks. In fact, MRI networks exhibit unique, subject-specific, patterns of connections, so that even within the same population, different individuals can show different network properties, such as degree distribution, which in turn can drive differences in modular structure (Fornito et al., 2013; Rubinov and Sporns, 2010; van Wijk et al., 2010). Our ensemble-based strategy, in which a network average is computed many times on a small subset of subjects, offers a solution to link changes of structural connectivity specifically to development, maturation, and aging processes, while minimizing the impact of individual differences not due to age. Therefore, it also overcomes the problem of heterogeneity in the age distribution of the sample. Moreover, thanks to the large data sample, we could build a multilayer network where layers represent narrow age intervals (2 years), so that we also avoided comparing modular structure across large age groups (usually children, adults, and elderly participants) that are internally highly heterogeneous. Instead, we could monitor modules' properties over an extended period of the lifespan.

To track the evolution of modules across the lifespan, we adopted a multilayer community detection algorithm (Mucha et al., 2010) that identifies assortative communities. While this is only one possible way of representing network organization, previous studies did suggest that

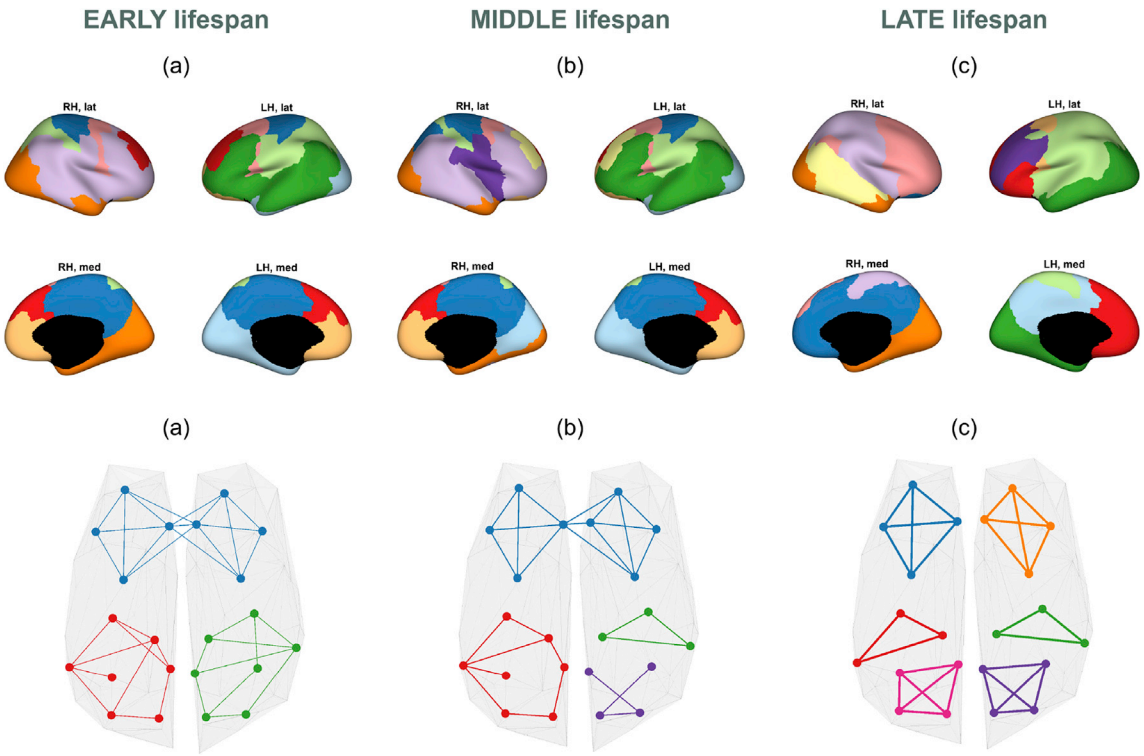

Fig. 8. Representative partitions (first row, panels a to c) and toy model (second row, panels d to f) of the modular structure of the brain connectome in three phases: early, middle and late lifespan. Different colors indicate different clusters. In the toy model the thickness of the edges is proportional to their weights.

modular architecture represents a neurobiologically meaningful aspect of brain connectivity (Sporns and Betzel, 2016), and it has been useful to describe learning processes (Bassett et al., 2011b), inter- and intra-subject variability (Betzel et al., 2019), differences among clinical cohorts (He et al., 2018), or model the brain network's dynamics (Khambhati et al., 2018). Our multilayer approach has the advantage of partitioning all the network's slices simultaneously, providing consistent partitioning of nodes across the layers and facilitating comparison of modules. Indeed, these are matched so that one can determine which brain regions change modular allegiance and in which period in the lifespan. Hence, rather than working independently on snapshots, this unified framework is more suitable to monitor age-related modules variations.

Community detection algorithms, including the Louvain algorithm adopted here, have stochastic properties that result in outputs with increasing heterogeneity as the size of the network increases, and can exhibit degeneracies (Good et al., 2010). Proposed solutions to this issue include consensus clustering (Lancichinetti and Fortunato, 2012), which produces an agreement among a set of partitions, or selecting a near-optimal representative partition. Here, we pursued an ensemble-based resampling approach. Instead of applying the algorithm multiple times on a given network and then selecting a partition, we applied it once for each member of a set of equivalent multilayer networks, and we statistically described the ensemble of output partitions, focusing on statistical consistency. This approach aims to highlight meaningful trends and mitigate variations due to chance, which can be encountered relying on a single representation of community structure. In each figure of the manuscript, we reported the average values of the investigated indices together with their confidence interval. These intervals barely deviate from the average values, meaning that the partitions and their structural properties, even if not identical, are quite consistent across the iterations. Robustness and statistical consistency are also promoted by the large sample size of participants. Previous work characterizing connectome during development showed discordant results, such as increasing (Chen et al., 2013) decreasing (Huang et al., 2015) or no change of modularity (Hagmann et al., 2010), possibly due to small sample sizes. Overall, we aimed for robust results through a large sample, a stringent resampling scheme and a multilayer approach that reinforces the analysis.

By optimizing multilayer modularity, we explored the connectome's architecture at multiple spatial and temporal scales, as evidence suggests that the human brain network can be parsed in several – physiologically equally meaningful – ways (Betzel et al., 2013; Betzel and Bassett, 2017). However, after having obtained modules with different sizes and degrees of variability across layers, we focused on a specific subset. We were interested in modules that reconfigure in an intermediate time scale, neither too fast nor too slow. To identify a proper scale, we considered the VI matrix (Fig. 2), which we hypothesized should have high similarity between partitions on the main diagonal and lower values outside. We also focused on a single spatial scale. While there is no exact number of modules with which brain networks must be divided, current practice has converged onto a set of functional modules which are reliably observed (Damoiseaux et al., 2006; Power et al., 2011; Thomas Yeo et al., 2011). They usually include the visual, somatomotor, dorsal attention, limbic, default mode, control and salience systems. Previous works demonstrated that structural and functional connectivity matrices are significantly related (Fukushima et al., 2018; Goñi et al., 2014), supporting the notion that structural connectivity underpins and drives functional organization. For this reason, we focused on a spatial scale that returned a number of modules consistent with canonical functional systems, which have also been identified in a previous analysis of structural connectivity (Faskowitz et al., 2018). All the findings we presented have to be seen in relation to this choice. We acknowledge that the choice of different temporal/spatial scales could lead to different properties of the age-related brain community organization.

4.3. Limitations and future advancements

There are several limitations inherent in MRI data. Diffusion imaging and tractography provide an estimation of the anatomical connectivity,

but not a direct measurement of it (Sotiropoulos and Zalesky, 2019). Through our approach to network construction and the multi-layer resampling methodology, we tried to ameliorate some biases such as the paucity of long-range connections detected with tractography data.

Another issue regards the node definition, as this choice might impact the properties of the derived network (Fornito et al., 2010). In order to be consistent with previous studies (Betzel et al., 2015, 2014; Cao et al., 2014; Faskowitz et al., 2018), we used a parcellation of the cortex based on a canonical partition of the surface into functional sub-systems (Thomas Yeo et al., 2011). To add robustness to our findings, future works could replicate the same analysis with a finer parcellation, or by defining nodes according to anatomical constraints (Destrieux et al., 2010).

While our study included much of the human lifespan, it did not cover early postnatal stages of development (ages 0–5 years). This period is characterized by rapid anatomical growth and behavioral/cognitive changes that we expect to be reflected in the topology of brain connectivity. As more data covering this early lifespan period becomes available, our ensemble multi-layer approach could be extended to cover the human lifespan more fully and comprehensively.

Finally, now that we provided a description of the evolution of the community structure during the lifespan, these patterns could also be assessed for cohorts of clinical subjects. The goal would be assessing the impact of specific pathologies on developmental or aging processes and helping to identify targeted interventions. Further studies might also attempt to correlate connectional features with behavioral features and normalize interindividual variations in cognition relative to the actual developmental status.

5. Conclusion

In conclusion, we develop an ensemble multi-layer approach and provide evidence that the human brain exhibits age-dependent modular organization. The number of modules increases with age while their size decreases. The modularity of the partitions reaches the highest values in the early and in the late lifespan, whereas the opposite happens for the participation coefficient. We also found that the rate of the modules' reconfiguration increases with age, resulting in modules that are more restricted to single cortical hemispheres. Our findings broaden a body of literature aimed at understanding connectome evolution across lifespan, while the methods developed can be used to monitor variables of interest in structural and functional brain networks across other large datasets.

Data availability statement

Subject-level adjacency matrices are made available at https://doi.org/10.6084/m9.figshare.6983018.

Declaration of competing interest

The authors declare no conflicting interests.

CRediT authorship contribution statement

Maria Grazia Puxeddu: Conceptualization, Methodology, Formal analysis, Software, Writing - original draft. **Joshua Faskowitz:** Data curation, Methodology, Writing - review & editing. **Richard F. Betzel:** Methodology, Writing - review & editing. **Manuela Petti:** Methodology, Writing - review & editing. **Laura Astolfi:** Supervision, Funding acquisition, Writing - review & editing. **Olaf Sporns:** Conceptualization, Supervision, Funding acquisition, Writing - review & editing.

Acknowledgment

M.G.P. was supported by the Grant "Avvio alla ricerca 2018" (No. AR1181643680C682) and Grant for mobility of PhD students received by the University of Rome La Sapienza. L.A. and M.G.P. would like to acknowledge "Progetti di Ateneo 2017" (RM11715C82606455), "Progetti di Ateneo 2018" (RP11816436CDA44C), "Progetti di Ateneo 2019" (RM11916B88C3E2DE) and Stiftelsen Promobilia, Research Project DISCLOSE. O.S. was supported by NIH/NIMH grants 1R01MH122957-01, 1R01AT009036 and 1R01MH122957. This material is based upon work supported by the National Science Foundation Graduate Research Fellowship under Grant No. 1342962 (J.F.). This research was supported by Indiana University Office of the Vice President for Research Emerging Area of Research Initiative, Learning: Brains, Machine and Children.

Appendix A. Supplementary data

Supplementary data to this article can be found online at https://doi.org/10.1016/j.neuroimage.2020.116974.

References

Andrews-Hanna, J.R., Snyder, A.Z., Vincent, J.L., Lustig, C., Head, D., Raichle, M.E., Buckner, R.L., 2007. Disruption of large-scale brain systems in advanced aging. Neuron 56, 924–935. https://doi.org/10.1016/j.neuron.2007.10.038.

Backlund, V.-P., Saramäki, J., Pan, R.K., 2014. Effects of temporal correlations on cascades: threshold models on temporal networks. Phys. Rev. E 89, 062815. https://doi.org/10.1103/PhysRevE.89.062815.

Bassett, D.S., Brown, J.A., Deshpande, V., Carlson, J.M., Grafton, S.T., 2011a. Conserved and variable architecture of human white matter connectivity. Neuroimage 54, 1262–1279. https://doi.org/10.1016/j.neuroimage.2010.09.006.

Bassett, D.S., Porter, M.A., Wymbs, N.F., Grafton, S.T., Carlson, J.M., Mucha, P.J., 2013. Robust detection of dynamic community structure in networks. Chaos 23, 013142. https://doi.org/10.1063/1.4790830.

Bassett, D.S., Sporns, O., 2017. Network neuroscience. Nat. Neurosci. 20, 353–364. https://doi.org/10.1038/nn.4502.

Bassett, D.S., Wymbs, N.F., Porter, M.A., Mucha, P.J., Carlson, J.M., Grafton, S.T., 2011b. Dynamic reconfiguration of human brain networks during learning. Proc. Natl. Acad. Sci. Unit. States Am. 108, 7641–7646. https://doi.org/10.1073/pnas.1018985108.

Baum, G.L., Ciric, R., Roalf, D.R., Betzel, R.F., Moore, T.M., Shinohara, R.T., Kahn, A.E., Vandekar, S.N., Rupert, P.E., Quarmley, M., Cook, P.A., Elliott, M.A., Ruparel, K., Gur, R.E., Gur, R.C., Bassett, D.S., Satterthwaite, T.D., 2017. Modular segregation of structural brain networks supports the development of executive function in youth. Curr. Biol. 27, 1561–1572. https://doi.org/10.1016/j.cub.2017.04.051 e8.

Betzel, R.F., Bassett, D.S., 2018. Specificity and robustness of long-distance connections in weighted, interareal connectomes. Proc. Natl. Acad. Sci. Unit. States Am. 115, E4880–E4889. https://doi.org/10.1073/pnas.1720186115.

Betzel, R.F., Bassett, D.S., 2017. Multi-scale brain networks. NeuroImage Funct. Architect. Brain 160, 73–83. https://doi.org/10.1016/j.neuroimage.2016.11.006.

Betzel, R.F., Bertolero, M.A., Gordon, E.M., Gratton, C., Dosenbach, N.U.F., Bassett, D.S., 2019. The community structure of functional brain networks exhibits scale-specific patterns of inter- and intra-subject variability. Neuroimage. https://doi.org/10.1016/j.neuroimage.2019.07.003.

Betzel, R.F., Byrge, L., He, Y., Goñi, J., Zuo, X.-N., Sporns, O., 2014. Changes in structural and functional connectivity among resting-state networks across the human lifespan. Neuroimage 102, 345–357. https://doi.org/10.1016/j.neuroimage.2014.07.067.

Betzel, R.F., Griffa, A., Avena-Koenigsberger, A., Goñi, J., Thiran, J.-P., Hagmann, P., Sporns, O., 2013. Multi-scale community organization of the human structural connectome and its relationship with resting-state functional connectivity. Netw. Sci. 1, 353–373. https://doi.org/10.1017/nws.2013.19.

Betzel, R.F., Griffa, A., Hagmann, P., Mišić, B., 2018a. Distance-dependent consensus thresholds for generating group-representative structural brain networks. Netw. Neurosci. 3, 475–496. https://doi.org/10.1162/netn_a_00075.

Betzel, R.F., Medaglia, J.D., Bassett, D.S., 2018b. Diversity of meso-scale architecture in human and non-human connectomes. Nat. Commun. 9, 1–14. https://doi.org/10.1038/s41467-017-02681-z.

Betzel, R.F., Mišić, B., He, Y., Rumschlag, J., Zuo, X.-N., Sporns, O., 2015. Functional Brain Modules Reconfigure at Multiple Scales across the Human Lifespan arXiv: 1510.08045 [q-bio].

Blondel, V.D., Guillaume, J.-L., Lambiotte, R., Lefebvre, E., 2008. Fast unfolding of communities in large networks. J. Stat. Mech.: Theory Exp. P10008. https://doi.org/10.1088/1742-5468/2008/10/P10008.

Buckner, R.L., 2004. Memory and executive function in aging and AD: multiple factors that cause decline and reserve factors that compensate. Neuron 44, 195–208. https://doi.org/10.1016/j.neuron.2004.09.006.

Buckner, R.L., Sepulcre, J., Talukdar, T., Krienen, F.M., Liu, H., Hedden, T., Andrews-Hanna, J.R., Sperling, R.A., Johnson, K.A., 2009. Cortical hubs revealed by intrinsic functional connectivity: mapping, assessment of stability, and relation to alzheimer's disease. J. Neurosci. 29, 1860–1873. https://doi.org/10.1523/JNEUROSCI.5062-08.2009.

Bullmore, E., Sporns, O., 2009. Complex brain networks: graph theoretical analysis of structural and functional systems. Nat. Rev. Neurosci. 10, 186–198. https://doi.org/10.1038/nrn2575.

Byrge, L., Sporns, O., Smith, L.B., 2014. Developmental process emerges from extended brain–body–behavior networks. Trends Cognit. Sci. 18, 395–403. https://doi.org/10.1016/j.tics.2014.04.010.

Cao, M., Wang, J.-H., Dai, Z.-J., Cao, X.-Y., Jiang, L.-L., Fan, F.-M., Song, X.-W., Xia, M.-R., Shu, N., Dong, Q., Milham, M.P., Castellanos, F.X., Zuo, X.-N., He, Y., 2014. Topological organization of the human brain functional connectome across the lifespan. Dev. Cognit. Neurosci. 7, 76–93. https://doi.org/10.1016/j.dcn.2013.11.004.

Cardillo, A., Petri, G., Nicosia, V., Sinatra, R., Gómez-Gardeñes, J., Latora, V., 2014. Evolutionary dynamics of time-resolved social interactions. Phys. Rev. E 90, 052825. https://doi.org/10.1103/PhysRevE.90.052825.

Chan, M.Y., Park, D.C., Savalia, N.K., Petersen, S.E., Wig, G.S., 2014. Decreased segregation of brain systems across the healthy adult lifespan. Proc. Natl. Acad. Sci. Unit. States Am. 111, E4997–E5006. https://doi.org/10.1073/pnas.1415122111.

Chen, Z., Liu, M., Gross, D.W., Beaulieu, C., 2013. Graph theoretical analysis of developmental patterns of the white matter network. Front. Hum. Neurosci. 7 https://doi.org/10.3389/fnhum.2013.00716.

Chen, Z.J., He, Y., Rosa-Neto, P., Gong, G., Evans, A.C., 2011. Age-related alterations in the modular organization of structural cortical network by using cortical thickness from MRI. Neuroimage 56, 235–245. https://doi.org/10.1016/j.neuroimage.2011.01.010.

Damoiseaux, J.S., Rombouts, S.a.R.B., Barkhof, F., Scheltens, P., Stam, C.J., Smith, S.M., Beckmann, C.F., 2006. Consistent resting-state networks across healthy subjects. Proc. Natl. Acad. Sci. Unit. States Am. 103, 13848–13853. https://doi.org/10.1073/pnas.0601417103.

De Domenico, M., 2017. Multilayer modeling and analysis of human brain networks. GigaScience 6. https://doi.org/10.1093/gigascience/gix004.

Dennis, E.L., Jahanshad, N., McMahon, K.L., de Zubicaray, G.I., Martin, N.G., Hickie, I.B., Toga, A.W., Wright, M.J., Thompson, P.M., 2013. Development of brain structural connectivity between ages 12 and 30: a 4-Tesla diffusion imaging study in 439 adolescents and adults. Neuroimage 64, 671–684. https://doi.org/10.1016/j.neuroimage.2012.09.004.

Destrieux, C., Fischl, B., Dale, A., Halgren, E., 2010. Automatic parcellation of human cortical gyri and sulci using standard anatomical nomenclature. Neuroimage 53, 1–15. https://doi.org/10.1016/j.neuroimage.2010.06.010.

Di Martino, A., Fair, D.A., Kelly, C., Satterthwaite, T.D., Castellanos, F.X., Thomason, M.E., Craddock, R.C., Luna, B., Leventhal, B.L., Zuo, X.-N., Milham, M.P., 2014. Unraveling the miswired connectome: a developmental perspective. Neuron 83, 1335–1353. https://doi.org/10.1016/j.neuron.2014.08.050.

Duffau, H., 2014. The huge plastic potential of adult brain and the role of connectomics: new insights provided by serial mappings in glioma surgery. Cortex 58, 325–337. https://doi.org/10.1016/j.cortex.2013.08.005.

Efron, B., Tibshirani, R.J., 1993. An Introduction to the Bootstrap. Springer US, Boston, MA. https://doi.org/10.1007/978-1-4899-4541-9.

Eickhoff, S.B., Paus, T., Caspers, S., Grosbras, M.-H., Evans, A.C., Zilles, K., Amunts, K., 2007. Assignment of functional activations to probabilistic cytoarchitectonic areas revisited. Neuroimage 36, 511–521. https://doi.org/10.1016/j.neuroimage.2007.03.060.

Faskowitz, J., Yan, X., Zuo, X.-N., Sporns, O., 2018. Weighted stochastic block models of the human connectome across the life span. Sci. Rep. 8, 12997. https://doi.org/10.1038/s41598-018-31202-1.

Filippi, M., van den Heuvel, M.P., Fornito, A., He, Y., Hulshoff Pol, H.E., Agosta, F., Comi, G., Rocca, M.A., 2013. Assessment of system dysfunction in the brain through MRI-based connectomics. Lancet Neurol. 12, 1189–1199. https://doi.org/10.1016/S1474-4422(13)70144-3.

Fornito, A., Zalesky, A., Breakspear, M., 2013. Graph analysis of the human connectome: promise, progress, and pitfalls. NeuroImage Mapp. Connectome 80, 426–444. https://doi.org/10.1016/j.neuroimage.2013.04.087.

Fornito, A., Zalesky, A., Bullmore, E.T., 2010. Network scaling effects in graph analytic studies of human resting-state fMRI data. Front. Syst. Neurosci. 4 https://doi.org/10.3389/fnsys.2010.00022.

Fortunato, S., 2010. Community detection in graphs. Phys. Rep. 486, 75–174. https://doi.org/10.1016/j.physrep.2009.11.002.

Fukushima, M., Betzel, R.F., He, Y., van den Heuvel, M.P., Zuo, X.-N., Sporns, O., 2018. Structure–function relationships during segregated and integrated network states of human brain functional connectivity. Brain Struct. Funct. 223, 1091–1106. https://doi.org/10.1007/s00429-017-1539-3.

Garyfallidis, E., Brett, M., Amirbekian, B., Rokem, A., Van Der Walt, S., Descoteaux, M., Nimmo-Smith, I., 2014. Dipy, a library for the analysis of diffusion MRI data. Front. Neuroinf. 8 https://doi.org/10.3389/fninf.2014.00008.

Girvan, M., Newman, M.E.J., 2002. Community structure in social and biological networks. Proc. Natl. Acad. Sci. U. S. A. 99, 7821–7826. https://doi.org/10.1073/pnas.122653799.

Gong, G., Rosa-Neto, P., Carbonell, F., Chen, Z.J., He, Y., Evans, A.C., 2009. Age- and gender-related differences in the cortical anatomical network. J. Neurosci. 29, 15684–15693. https://doi.org/10.1523/JNEUROSCI.2308-09.2009.

Goñi, J., van den Heuvel, M.P., Avena-Koenigsberger, A., Vélez de Mendizábal, N., Betzel, R.F., Griffa, A., Hagmann, P., Corominas-Murtra, B., Thiran, J.-P., Sporns, O., 2014. Resting-brain functional connectivity predicted by analytic measures of network communication. Proc. Natl. Acad. Sci. Unit. States Am. 111, 833–838. https://doi.org/10.1073/pnas.1315529111.

Good, B.H., de Montjoye, Y.-A., Clauset, A., 2010. Performance of modularity maximization in practical contexts. Phys. Rev. E 81, 046106. https://doi.org/10.1103/PhysRevE.81.046106.

Guimerà, R., Amaral, L.A.N., 2005. Functional cartography of complex metabolic networks. Nature 433, 895. https://doi.org/10.1038/nature03288.

Hagmann, P., Sporns, O., Madan, N., Cammoun, L., Pienaar, R., Wedeen, V.J., Meuli, R., Thiran, J.-P., Grant, P.E., 2010. White matter maturation reshapes structural connectivity in the late developing human brain. Proc. Natl. Acad. Sci. Unit. States Am. 107, 19067–19072. https://doi.org/10.1073/pnas.1009073107.

He, Y., Lim, S., Fortunato, S., Sporns, O., Zhang, L., Qiu, J., Xie, P., Zuo, X.-N., 2018. Reconfiguration of cortical networks in MDD uncovered by multiscale community detection with fMRI. Cerebr. Cortex 28, 1383–1395. https://doi.org/10.1093/cercor/bhx335.

Holme, P., 2015. Modern temporal network theory: a colloquium. Eur. Phys. J. B 88, 234. https://doi.org/10.1140/epjb/e2015-60657-4.

Holme, P., Saramäki, J., 2012. Temporal networks. Physics reports. Temporal Netw. 519, 97–125. https://doi.org/10.1016/j.physrep.2012.03.001.

Huang, H., Shu, N., Mishra, V., Jeon, T., Chalak, L., Wang, Z.J., Rollins, N., Gong, G., Cheng, H., Peng, Y., Dong, Q., He, Y., 2015. Development of human brain structural networks through infancy and childhood. Cerebr. Cortex 25, 1389–1404. https://doi.org/10.1093/cercor/bht335.

Imperati, D., Colcombe, S., Kelly, C., Martino, A.D., Zhou, J., Castellanos, F.X., Milham, M.P., 2011. Differential development of human brain white matter tracts. PloS One 6, e23437. https://doi.org/10.1371/journal.pone.0023437.

Jutla, I.S., Jeub, L.G.S., Mucha, P.J., n.d. A Generalized Louvain Method for Community Detection Implemented in Matlab 2.

Kelly, C., Biswal, B.B., Craddock, R.C., Castellanos, F.X., Milham, M.P., 2012. Characterizing variation in the functional connectome: promise and pitfalls. Trends Cognit. Sci. 16, 181–188. https://doi.org/10.1016/j.tics.2012.02.001.

Khambhati, A.N., Sizemore, A.E., Betzel, R.F., Bassett, D.S., 2018. Modeling and interpreting mesoscale network dynamics. NeuroImage Brain Connect. Dynam. 180, 337–349. https://doi.org/10.1016/j.neuroimage.2017.06.029.

Kivelä, M., Arenas, A., Barthelemy, M., Gleeson, J.P., Moreno, Y., Porter, M.A., 2014. Multilayer networks. J. Complex Netw. 2, 203–271. https://doi.org/10.1093/comnet/cnu016.

Lancichinetti, A., Fortunato, S., 2012. Consensus clustering in complex networks. Sci. Rep. 2, 336. https://doi.org/10.1038/srep00336.

Lebel, C., Gee, M., Camicioli, R., Wieler, M., Martin, W., Beaulieu, C., 2012. Diffusion tensor imaging of white matter tract evolution over the lifespan. Neuroimage 60, 340–352. https://doi.org/10.1016/j.neuroimage.2011.11.094.

Lim, S., Han, C.E., Uhlhaas, P.J., Kaiser, M., 2015. Preferential detachment during human brain development: age- and sex-specific structural connectivity in diffusion tensor imaging (DTI) data. Cerebr. Cortex 25, 1477–1489. https://doi.org/10.1093/cercor/bht333.

Meilă, M., 2007. Comparing clusterings—an information based distance. J. Multivariate Anal. 98, 873–895. https://doi.org/10.1016/j.jmva.2006.11.013.

Mucha, P.J., Richardson, T., Macon, K., Porter, M.A., Onnela, J.-P., 2010. Community structure in time-dependent, multiscale, and multiplex networks. Science 328, 876–878. https://doi.org/10.1126/science.1184819.

Muldoon, S.F., Bassett, D.S., 2016. Network and multilayer network approaches to understanding human brain dynamics. https://doi.org/10.1086/687857.

Newman, M.E.J., 2012. Communities, modules and large-scale structure in networks. Nat. Phys. 8, 25–31. https://doi.org/10.1038/nphys2162.

Newman, M.E.J., Girvan, M., 2004. Finding and evaluating community structure in networks. Phys. Rev. 69 https://doi.org/10.1103/PhysRevE.69.026113.

Nooner, K.B., Colcombe, S., Tobe, R., Mennes, M., Benedict, M., Moreno, A., Panek, L., Brown, S., Zavitz, S., Li, Q., Sikka, S., Gutman, D., Bangaru, S., Schlachter, R.T., Kamiel, S., Anwar, A., Hinz, C., Kaplan, M., Rachlin, A., Adelsberg, S., Cheung, B., Khanuja, R., Yan, C., Craddock, C., Calhoun, V., Courtney, W., King, M., Wood, D., Cox, C., Kelly, C., DiMartino, A., Petkova, E., Reiss, P., Duan, N., Thompsen, D., Biswal, B., Coffey, B., Hoptman, M., Javitt, D.C., Pomara, N., Sidtis, J., Koplewicz, H., Castellanos, F.X., Leventhal, B., Milham, M., 2012. The NKI-Rockland sample: a model for accelerating the pace of discovery science in psychiatry. Front. Neurosci. 6 https://doi.org/10.3389/fnins.2012.00152.

Pan, R.K., Saramäki, J., 2011. Path lengths, correlations, and centrality in temporal networks. Phys. Rev. E 84, 016105. https://doi.org/10.1103/PhysRevE.84.016105.

Persson, J., Nyberg, L., Lind, J., Larsson, A., Nilsson, L.-G., Ingvar, M., Buckner, R.L., 2006. Structure–function correlates of cognitive decline in aging. Cerebr. Cortex 16, 907–915. https://doi.org/10.1093/cercor/bhj036.

Petti, M., Toppi, J., Babiloni, F., Cincotti, F., Mattia, D., Astolfi, L., 2016. EEG Resting-State Brain Topological Reorganization as a Function of Age.

Porter, M.A., Onnela, J.-P., Mucha, P.J., 2009. Communities in Networks (SSRN Scholarly Paper No. ID 1357925). Social Science Research Network, Rochester, NY.

Power, J.D., Cohen, A.L., Nelson, S.M., Wig, G.S., Barnes, K.A., Church, J.A., Vogel, A.C., Laumann, T.O., Miezin, F.M., Schlaggar, B.L., Petersen, S.E., 2011. Functional network organization of the human brain. Neuron 72, 665–678. https://doi.org/10.1016/j.neuron.2011.09.006.

Raz, N., Ghisletta, P., Rodrigue, K.M., Kennedy, K.M., Lindenberger, U., 2010. Trajectories of brain aging in middle-aged and older adults: regional and individual differences. Neuroimage 51, 501–511. https://doi.org/10.1016/j.neuroimage.2010.03.020.

Rubinov, M., Sporns, O., 2010. Complex network measures of brain connectivity: uses and interpretations. NeuroImage Comput. Models Brain 52, 1059–1069. https://doi.org/10.1016/j.neuroimage.2009.10.003.

Sambataro, F., Murty, V.P., Callicott, J.H., Tan, H.-Y., Das, S., Weinberger, D.R., Mattay, V.S., 2010. Age-related alterations in default mode network: impact on working memory performance. Neurobiol. Aging 31, 839–852. https://doi.org/10.1016/j.neurobiolaging.2008.05.022.

Schaub, M.T., Delvenne, J.-C., Rosvall, M., Lambiotte, R., 2017. The many facets of community detection in complex networks. Appl. Netw. Sci. 2, 1–13. https://doi.org/10.1007/s41109-017-0023-6.

Sinke, M.R.T., Dijkhuizen, R.M., Caimo, A., Stam, C.J., Otte, W.M., 2016. Bayesian exponential random graph modeling of whole-brain structural networks across lifespan. Neuroimage 135, 79–91. https://doi.org/10.1016/j.neuroimage.2016.04.066.

Sotiropoulos, S.N., Zalesky, A., 2019. Building connectomes using diffusion MRI: why, how and but. NMR Biomed. 32, e3752 https://doi.org/10.1002/nbm.3752.

Sporns, O., 2014. Contributions and challenges for network models in cognitive neuroscience. Nat. Neurosci. 17, 652–660. https://doi.org/10.1038/nn.3690.

Sporns, O., 2011. The human connectome: a complex network. Ann. N. Y. Acad. Sci. 1224, 109–125. https://doi.org/10.1111/j.1749-6632.2010.05888.x.

Sporns, O., Betzel, R.F., 2016. Modular brain networks. Annu. Rev. Psychol. 67, 613–640. https://doi.org/10.1146/annurev-psych-122414-033634.

Starnini, M., Baronchelli, A., Barrat, A., Pastor-Satorras, R., 2012. Random walks on temporal networks. Phys. Rev. E 85, 056115. https://doi.org/10.1103/PhysRevE.85.056115.

Thomas Yeo, B.T., Krienen, F.M., Sepulcre, J., Sabuncu, M.R., Lashkari, D., Hollinshead, M., Roffman, J.L., Smoller, J.W., Zöllei, L., Polimeni, J.R., Fischl, B., Liu, H., Buckner, R.L., 2011. The organization of the human cerebral cortex estimated by intrinsic functional connectivity. J. Neurophysiol. 106, 1125–1165. https://doi.org/10.1152/jn.00338.2011.

Vaiana, M., Muldoon, S.F., 2018. Multilayer brain networks. J. Nonlinear Sci. https://doi.org/10.1007/s00332-017-9436-8.

van Wijk, B.C.M., Stam, C.J., Daffertshofer, A., 2010. Comparing brain networks of different size and connectivity density using graph theory. PloS One 5, e13701. https://doi.org/10.1371/journal.pone.0013701.

Westlye, L.T., Walhovd, K.B., Dale, A.M., Bjørnerud, A., Due-Tønnessen, P., Engvig, A., Grydeland, H., Tamnes, C.K., Østby, Y., Fjell, A.M., 2010. Life-span changes of the human brain white matter: diffusion tensor imaging (DTI) and volumetry. Cerebr. Cortex 20, 2055–2068. https://doi.org/10.1093/cercor/bhp280.

Wu, K., Taki, Y., Sato, K., Kinomura, S., Goto, R., Okada, K., Kawashima, R., He, Y., Evans, A.C., Fukuda, H., 2012. Age-related changes in topological organization of structural brain networks in healthy individuals. Hum. Brain Mapp. 33, 552–568. https://doi.org/10.1002/hbm.21232.

Yeatman, J.D., Wandell, B.A., Mezer, A.A., 2014. Lifespan maturation and degeneration of human brain white matter. Nat. Commun. 5, 4932. https://doi.org/10.1038/ncomms5932.

Zhou, J., Gennatas, E.D., Kramer, J.H., Miller, B.L., Seeley, W.W., 2012. Predicting regional neurodegeneration from the healthy brain functional connectome. Neuron 73, 1216–1227. https://doi.org/10.1016/j.neuron.2012.03.004.

Zuo, X.-N., He, Y., Betzel, R.F., Colcombe, S., Sporns, O., Milham, M.P., 2017. Human connectomics across the life span. Trends Cognit. Sci. 21, 32–45. https://doi.org/10.1016/j.tics.2016.10.005.